Copper Coordination in the Full-Length, Recombinant Prion Protein†

Colin S. Burns,[‡,#] Eliah Aronoff-Spencer,[§,#] Giuseppe Legname,[||] Stanley B. Prusiner,[||,⊥] William E. Antholine,[$] Gary J. Gerfen,[§] Jack Peisach,[§] and Glenn L. Millhauser*[,‡]

Department of Chemistry and Biochemistry, University of California, Santa Cruz, California 95064, Department of Physiology and Biophysics, Albert Einstein College of Medicine, Bronx, New York 10461, Institute for Neurodegenerative Diseases and Departments of Neurology and of Biochemistry and Biophysics, University of California, San Francisco, California 94143, and Biophysics Research Institute, Medical College of Wisconsin, Milwaukee, Wisconsin 53226

Received November 8, 2002; Revised Manuscript Received March 20, 2003

ABSTRACT: The prion protein (PrP) binds divalent copper at physiologically relevant conditions and is believed to participate in copper regulation or act as a copper-dependent enzyme. Ongoing studies aim at determining the molecular features of the copper binding sites. The emerging consensus is that most copper binds in the octarepeat domain, which is composed of four or more copies of the fundamental sequence PHGGGWGQ. Previous work from our laboratory using PrP-derived peptides, in conjunction with EPR and X-ray crystallography, demonstrated that the HGGGW segment constitutes the fundamental binding unit in the octarepeat domain [Burns et al. (2002) *Biochemistry 41*, 3991−4001; Aronoff-Spencer et al. (2000) *Biochemistry 39*, 13760−13771]. Copper coordination arises from the His imidazole and sequential deprotonated glycine amides. In this present work, recombinant, full-length Syrian hamster PrP is investigated using EPR methodologies. Four copper ions are taken up in the octarepeat domain, which supports previous findings. However, quantification studies reveal a fifth binding site in the flexible region between the octarepeats and the PrP globular C-terminal domain. A series of PrP peptide constructs show that this site involves His96 in the PrP(92−96) segment GGGTH. Further examination by X-band EPR, S-band EPR, and electron spin−echo envelope spectroscopy, demonstrates coordination by the His96 imidazole and the glycine preceding the threonine. The copper affinity for this type of binding site is highly pH dependent, and EPR studies here show that recombinant PrP loses its affinity for copper below pH 6.0. These studies seem to provide a complete profile of the copper binding sites in PrP and support the hypothesis that PrP function is related to its ability to bind copper in a pH-dependent fashion.

Prion diseases are fatal neurodegenerative disorders of both humans and animals (*1*). The causative agent is an isoform of a normal, host-encoded membrane glycoprotein called the prion protein (PrP).[1] The normal cellular isoform (PrP^C) is the precursor to the pathogenic, protease-resistant isoform termed PrP^{Sc}, which is responsible for homologous pathologies within its individual hosts. With rare but notable exceptions, prion diseases respect the species barrier (*2*, *3*). Among these exceptions is the transmission of disease from scrapie-infected sheep to cattle, producing bovine spongiform encephalopathy (BSE) with subsequent penetration into the human population as variant Creutzfeldt-Jakob disease (vCJD) (*4*).

PrP^C is found in all mammals and avian species, yet its normal physiological function has not as yet been determined. However, the recently discovered ability of PrP^C to bind divalent copper (Cu^{2+}) in vivo and in vitro suggests that its normal function is related to copper homeostasis or to copper-dependent enzyme function (*5*−*13*). One recent study finds that Cu^{2+} stimulates PrP endocytosis, perhaps suggesting that the role of PrP^C is to shuttle Cu^{2+} from the synaptic space to the cell interior (*14*). A subsequent study showed, however, that cuproenzyme activity was not influenced by the degree of PrP expression in brain tissue, in turn leading the authors to suggest that PrP^C may act as a reversible sink or carrier of the metal ion (*15*). It has also been proposed that PrP^C functions as a superoxide dismutase (SOD), protecting synaptic regions from oxidative stress (*16*, *17*). Regardless of the specific function yet to be discovered, these ideas lead to the intriguing hypothesis that loss of normal PrP^C function may participate in neurodegeneration in prion disease (*16*, *18*).

The tertiary structures of recombinant unglycosylated human, mouse, and hamster PrP^C have been determined by NMR (*19*−*22*). Under Cu^{2+}-free conditions, the N-terminal portion of mature PrP^C, residues 23−125, is largely unstructured while the C-terminal segment, residues 126−231,

† This work was supported by NIH Grants GM 65790 (G.L.M.), GM 60609 (G.J.G.), GM 40168 (J.P.), AG02132 and AG10770 (S.B.P.).

* Corresponding author. Telephone: (831) 459-2176. Fax: (831) 459−2935. E-mail: glennm@hydrogen.ucsc.edu.

[#] These authors made equal contributions to this work.

[‡] Department of Chemistry & Biochemistry, UC Santa Cruz.

[§] Albert Einstein College of Medicine.

[||] Institute for Neurodegenerative Diseases, Department of Neurology, UC San Francisco.

[⊥] Department of Biochemistry and Biophysics, UC San Francisco.

[$] Medical College of Wisconsin.

[1] Abbreviations: PrP, prion protein; PrP^C, cellular isoform of PrP; PrP^{Sc}, scrapie isoform of PrP; rSHaPrP, recombinant Syrian hamster PrP; rMoPrP, recombinant mouse PrP; PrP(57−91), residues 57−91 of PrP; BSE, bovine spongiform encephalopathy; vCJD, variant Creutzfeldt-Jakob disease; SOD, superoxide dismutase; EPR, electron paramagnetic resonance; CW EPR, continuous wave EPR; ESEEM, electron spin−echo envelope modulation; K_d, dissociation constant; CD, circular dichroism; NMR, nuclear magnetic resonance; XAFS, X-ray absorption fine structure; DEPC, diethylpyrocarbonate.

10.1021/bi027138+ CCC: $25.00
Published on Web 05/15/2003

adopts a globular fold composed of three α-helices and two short β-strands. It is now recognized that most Cu^{2+} binding takes place in the PrP^C N-terminal region, which, in most humans, contains four sequential copies of a highly conserved octarepeat sequence PHGGGWGQ spanning residues 60−91. Several studies have shown that this segment selectively binds Cu^{2+} over other divalent metal ion species (*8*, *11*, *23*, *24*).

Using EPR, CD, and X-ray crystallography, we recently investigated the mode of Cu^{2+} binding in the PrP octarepeat domain (*9*, *10*). Consistent with most other studies, we found a Cu^{2+}/octarepeat stoichiometry of 1:1 at pH > 7. At reduced pH, the octarepeat domain loses its affinity for copper, consistent with the proposal that PrP may function as a sensor or transporter that operates through PrP endocytosis. Our studies further demonstrated that the peptide unit HGGGW, contained in each octarepeat sequence, is the fundamental Cu^{2+} binding site. Within the HGGGW segment, copper is coordinated by a nitrogen of the His imidazole, two deprotonated backbone nitrogens from the following glycines, and the amide carbonyl of the second glycine (*10*). In addition, the Trp indole hydrogen bonds to an axially coordinated water molecule (*10*). When fully copper-loaded, each HGGGW unit binds a single Cu^{2+} and is separated from the next Cu^{2+}-HGGGW segment by an intervening Gly−Gln−Pro linkage. Amide coordination is pH sensitive and thus explains why PrP loses its affinity for copper below pH 6.

Here we focus on the interaction of copper with full-length recombinant PrP. There are two goals of this present study. First, we wish to examine whether the binding mode and stoichiometry identified using peptides derived from the octarepeat domain is the same in the full-length protein. Second, there have been reports suggesting that PrP contains an additional copper binding site outside of the octarepeat domain; we therefore seek to use EPR methods to identify and characterize this site. Comparative experiments performed on full-length rSHaPrP and rSHaPrP(90−231), devoid of the octarepeat domain, indeed corroborates previous stoichiometry studies showing that full-length protein binds approximately five copper ions per protein with one of the copper sites outside of the octarepeat domain (*12*, *13*). Variable pH studies demonstrate that recombinant PrP exhibits affinity for copper only above pH 6.0, as found with octarepeat peptides. Next, using a series of peptide constructs, along with S-band EPR and electron spin−echo envelope modulation (ESEEM), we mapped specific Cu^{2+} contacts in the site outside of the octarepeat domain. Interestingly, although this specific copper site may bind independently, it demonstrates a unique ability to influence the cooperative binding of the entire N-terminal copper binding region (*5*). In conjunction with previous work, this present study advances the understanding of the molecular features of the copper binding sites in full-length recombinant PrP and thus may provide an essential foundation for evaluating the normal physiological function of the prion protein.

MATERIAL AND METHODS

Peptide Synthesis. All peptides were prepared with an acetyl group at the N-terminus and amidated at the C-terminus. Methods for synthesis, purification, and characterization have been described previously (*9*). N-Fmoc-glycine (^{15}N, 98+ %) was obtained from Cambridge Isotope Laboratories, Inc.

Protein Expression, Purification, and Refolding. Syrian hamster PrPs consisting of residues 29−231 and 90−231 were expressed in a protease-deficient *Escherichia coli* strain (27C7) under the control of the alkaline phosphatase promoter, as described elsewhere (*25*). The cells were homogenized by a microfluidizer (Microfluidics Corp.), and the insoluble fraction containing rPrP was pelleted by centrifugation. The pellet was solubilized in 8 M Gdn·HCl and 100 mM DTT. The solubilized material was purified by size exclusion chromatography in 6 M Gdn·HCl, 1 mM EDTA, and 50 mM Tris-HCl, pH 8 and then reverse-phase chromatography using a C4 column (Vydac) with an acetonitrile/water gradient. The pooled fractions containing rPrP were lyophilized and then solubilized in 8 M Gdn·HCl. For refolding, these samples were diluted to a final concentration of 100 μg/mL in 25 mM Tris-acetate, pH 8, and 5 mM EDTA. The solution was dialyzed against 20 mM sodium acetate, pH 5.5, and 0.05% NaN_3 and concentrated by ultrafiltration. Prior to use in experiments, protein solutions were spun in a microcentrifuge for 20 min and the supernatant was passed through a 0.02 μm Whatman Anatop filter. The filtered solution was then used immediately.

To ensure that rSHaPrP(29−231) remained properly folded in the buffer used for EPR experiments, CD spectra were acquired on an Aviv 60DS spectrometer at 291 K. A 0.1-cm path length cell was used for spectra recorded between 200 and 260 nm, sampling points every 1.0 or 0.5 nm. The CD spectrum of rSHaPrP(29−231) in 25 mM *N*-ethylmorpholine (NEM) and 20% glycerol (v/v) pH 5.5 (data not shown) is nearly identical to that reported by Stöckel et al. in both spectral shape and mean residue molar ellipticity (*11*). The conditions used for the latter CD were 4 μM rSHaPrP(29−231) in 50 mM sodium acetate at pH 6. Raising the pH to 7.4 does not alter the CD spectrum although the solubility of rSHaPrP(29−231) decreases significantly. To ensure that glycerol did not adversely affect the secondary structure, the CD of rSHaPrP(29−231) was obtained in 25 mM *N*-ethylmorpholine buffer pH 5.5 and reproduced the results for the experiment with 20% glycerol.

Protein and Peptide Concentration Determination. Concentrations were determined by aquiring UV−Vis spectra of samples in 6 M guanidine hydrochloride. The extinction coefficient for tryptophan at 280 nm was taken to be 5609 M^{-1} cm^{-1}. The extinction coefficients for GGGTH and PrP(106−116) at 214 nm in 6 M guanidine hydrochloride were determined, by amino acid analysis, to be 7914 and 13 407 M^{-1} cm^{-1}, respectively. The Molecular Structure Facility at the University of California, Davis, performed amino acid analysis.

Electron Paramagnetic Resonance (EPR) Spectroscopy. All samples were prepared with degassed buffer containing 25 mM NEM and 20% glycerol (v/v) in which the glycerol served as a cryoprotectant. X-band spectra (9.43 GHz) were acquired using a Bruker ESP380 spectrometer and a TE_{102} cavity equipped with variable temperature control. ^{63}Cu (99.62%, Cambridge Isotope Laboratories) was used to avoid inhomogeneous broadening of the S-band EPR lines that would otherwise be present with the mixture of naturally occurring isotopes. S-band spectra (3.5 GHz) were acquired in D_2O solution at 133 K using a loop gap resonator as part

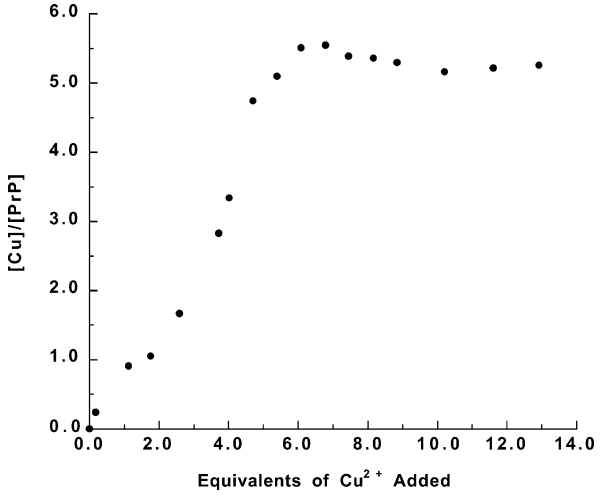

FIGURE 1: Integrated EPR signal intensity as a function of titrated Cu^{2+} at pH 7.4 for rSHaPrP(29−231). The protein concentration is 21 μm, and the copper ion concentration is reported in equivalents per protein. All data collected at 85 K.

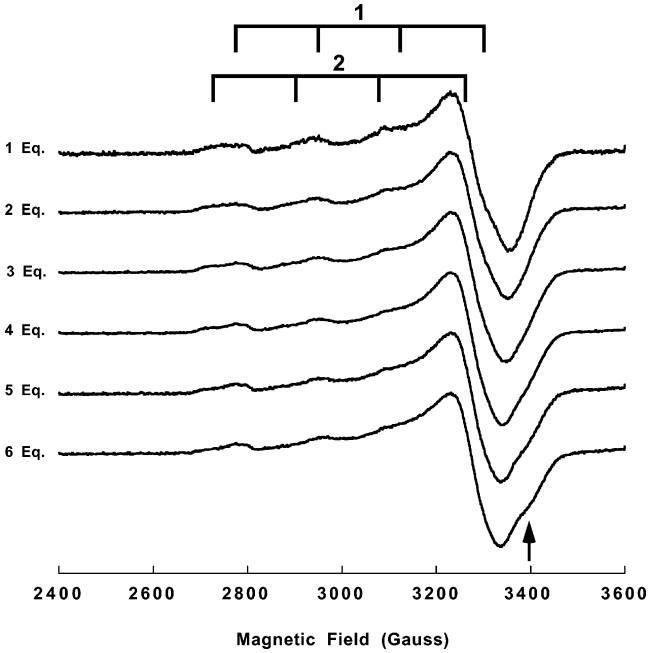

FIGURE 2: X-band EPR spectra of 21 μm rSHaPrP(29−231) with varying equivalents of Cu^{2+} at pH 7.4. The two different species are indicated with numbered grids at top, where 1 highlights the dominant signal at high Cu^{2+} load and 2 highlights the signal present at low Cu^{2+} load. The arrow at bottom indicates the region where an addition feature is present at 5 and 6 equiv of added Cu^{2+}. Each spectrum has been normalized to unit area. Spectra collected at 85 K, ν_0 = 9.43 GHz, and a sweep width of 1200 G.

of a specially designed spectrometer housed at the Biomedical ESR Center at the Medical College of Wisconsin. Three-pulse ESEEM measurements were obtained at 4.2 K on an X-band pulsed-EPR spectrometer. The instrument, cavity, and resonator were constructed in-house and have been previously described (*26*, *27*). Data were obtained at $g_\perp$, the point of greatest spectral intensity (3280 G at 9.47 GHz). Data processing to attain frequency domain spectra for 3-pulse ESEEM was carried out using software described in previous work (*28*). Experimental parameters for all pulsed experiments are provided in figure legends.

Determination of Cu^{2+} Binding Stoichiometry. Copper titrations were monitored by EPR in frozen solution at 85 K. Solutions of $CuCl_2$ were made in NEM buffer such that 5 μL additions would deliver the equivalents of copper necessary for the given titration. The pH of the copper stock was adjusted to 7.4 so that the pH of the peptide solution would not vary during the titration. The *x*-axis for the titration of each protein or peptide was generated by performing a standardizing titration of the Cu^{2+} solution into a 25 mM imidazole solution at pH 7.4. Under these conditions, all Cu^{2+} delivered by each titration step can be quantified. Copper concentrations were determined by comparison to a standard. End point concentrations, which were used to ascertain the binding equivalence, were aided by fitting the low and high [Cu^{2+}] regions of the curve to a linear function. The total bound Cu^{2+} was quantified by spin integration and comparison to accurate standard solutions containing Cu^{2+} in 10 mM imidazole at pH 7.4.

RESULTS

Cu^{2+} Quantification by EPR. Using methods developed previously (*9*), EPR spectra were obtained as a function of titrated Cu^{2+} to determine the metal ion to PrP binding stoichiometry. Titration results from a solution containing 21 μM rSHaPrP(29−231) at pH 7.4 are shown in Figure 1. The titration curve increases in an approximate linear fashion up to a saturation point along the *x*-axis at 5.9 ± 1.2 equiv of added copper. (Note that aqueous Cu^{2+} at pH 7.0 and above forms EPR silent $[Cu(OH)_2]_n$ and thus does not contribute to the observed spectrum or its integral (*9*).) To determine the amount of spin-active Cu^{2+} bound to rSHaPrP(29−231), quantitative spin integration was determined at each point. The result, shown as a ratio of Cu^{2+} to PrP along the *y*-axis, was found to be 5.3 ± 1.1 equiv of copper. The close agreement between the added copper and that detected by spin integration suggests that all of the bound copper is paramagnetic with little evidence for a diamagnetically coupled species. These data demonstrate that PrP binds between 5 and 6 equiv of Cu^{2+} at pH 7.4, a result that is in agreement with other studies (*12*, *13*), with no evidence of magnetic exchange interaction among the copper centers.

There are noticeable differences among the spectra of rSHaPrP(29−231) at low versus high Cu^{2+} load as shown in Figure 2. At 1 and 2 equiv of Cu^{2+}, the spectra consist of at least two distinct EPR signals. The feature with the highest parallel $g_{||}$ value loses intensity with additional Cu^{2+}. Interestingly, the titration behavior of rSHaPrP(29−231) closely parallels that of PrP(23−28,57−91), a peptide encompassing only the octarepeat domain (*9*). The observed spectral changes argue that at low Cu^{2+} concentrations, PrP^C coordinates copper in a manner that is distinct from that observed in the fully bound complex (*9*). Subtle changes in the $g_\perp$ region around 3400 G are apparent in rSHaPrP(29−231) at 5 and 6 equiv of Cu^{2+}.

To search for the location of the additional Cu^{2+} binding sites outside of the octarepeat domain, we examined rSHaPrP(90−231), which is composed of the flexible region beyond the octarepeats and the ordered PrP C-terminal domain. Spectra of a 157 μM protein solution as a function of added copper are shown in Figure 3. At 1.0 equiv of Cu^{2+}, rSHaPrP(90−231) binds 0.8 ± 0.2 equiv, giving rise to a spectrum with a significant negative peak on the high field edge of the perpendicular region. With continued addition

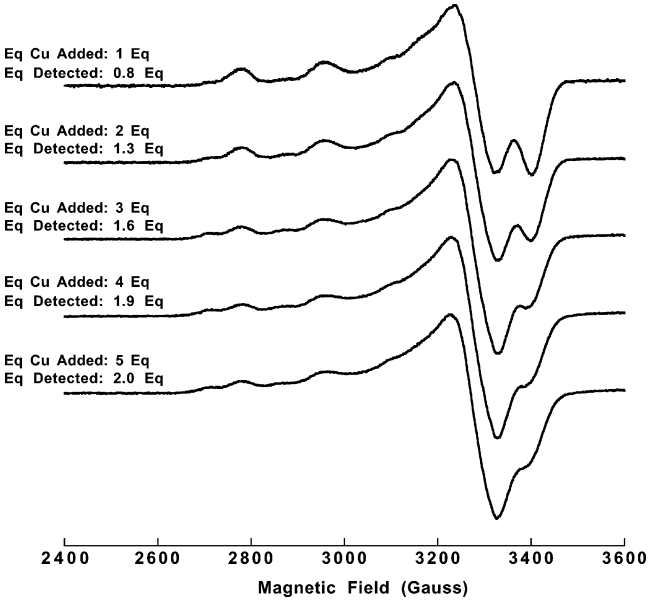

FIGURE 3: X-band EPR spectra of 157 μm rSHaPrP(90−231) with varying equivalents of Cu^{2+} at pH 7.4. Spectra collected at 85 K, $\upsilon_0 = 9.43$ GHz, and a sweep width of 1200 G.

Table 1: PrP-Derived Peptide Sequences

PrP(23−28,57−98)	KKRPKPWGQ(PHGGGWGQ)$_4$GGGTHNQ
PrP(23−28,57−91)	KKRPKPWGQ(PHGGGWGQ)$_4$
PrP(90−116)	GQGGGTHNQWNKPSKPKTNMKHMAGAA
PrP(90−101)	GQGGGTHNQWNK
PrP(106−116)	KTNMKHMAGAA
PrP(92−96)	GGGTH
PrP(94−96)	GTH

of Cu^{2+}, another signal emerges with a prominent minimum just above 3300 G. This species grows in slowly and does not saturate until approximately 5.0 equiv of Cu^{2+}. At this point, integration indicates that rSHaPrP(90−231) has taken up 2.0 equiv. Because the first site takes up added copper in a nearly quantitative fashion, the dissociation constant for this site is likely to be in the low micromolar range, as found with binding sites in the octarepeat domain. (Because of the rPrP and copper concentrations used, it is difficult to use EPR to quantify this specific dissociation constant. See ref *9*.) The second site, however, exhibits a much lower affinity. Using the EPR integration at 3.0 and 4.0 equiv, the Cu^{2+} dissociation constant was estimated to be approximately 500 μM. This affinity is probably too low to be of physiological significance and may reflect nonspecific binding, and thus further characterization of this site was not pursued. Taken together, these data demonstrate that rSHaPrP(90−231) binds a single additional copper ion with a micromolar affinity similar to that observed for the octarepeat domain (see also Table 2).

To identify the residues participating in the rSHaPrP(90−231) copper site, a series of peptides were prepared. These constructs, and PrP(23−28,57−91) from our previous studies, are listed in Table 1. Figure 4 shows the sequential relationship of these peptides and rSHaPrP(90−231) to full length PrP. Since polypeptide N-terminal amines can directly bind copper, all peptides were chemically blocked with an acetyl group (Ac) at the N-terminus. Further, the C-terminus of each peptide was protected as an amide to avoid a non-native backbone charge. The copper binding stoichiometry of these PrP-derived constructs are reported along with the results from the recombinant proteins in Table 2 and Figure 4. As reported previously, the octarepeat-containing peptide PrP(23−28,57−91) binds 3.8 ± 0.8 equiv of Cu^{2+} (*9*). PrP(23−28,57−98), composed of the octarepeat domain and the intervening region between the octarepeat domain and the globular C-terminus, binds 5.2 ± 1.0 equiv, consistent with the full-length protein. The histidine residue at position 96 most likely constitutes the focal point for the newly identified binding site outside of the octarepeat domain. The peptides PrP(90−116), PrP(90−101), PrP(106−116), and PrP(92−96) are C-terminal to residue 90, and, in the presence of excess metal ion, each coordinates approximately one equivalent of copper with the exception of PrP(90−116), which weakly binds an additional copper, consistent with the titration of rSHaPrP(90−231) (Table 2).

pH-Dependence of Cu^{2+} Binding. The interactions between Cu^{2+} and the PrP-derived peptides are strongly pH dependent. The X-band spectra of full-length rPrP, approximately 39 μM, with 6 equiv of Cu^{2+} at several pH values between 7.4 and 5.5 are shown in Figure 5. Examination of the spectra shows that as the pH is decreased, the low field hyperfine lines in the parallel region change significantly (Figure 5). The measured shifts in $g_{||}$ and $A_{||}$ reflect changes in the ligand environment of the copper ion. Starting at pH 7.40, the spectrum has three dominant peaks in the parallel region with $g_{||} = 2.22$ and $A_{||} = 541$ MHz (174 G). Reducing the pH to 7.06 and then 6.20, there is a decrease in intensity of the $g_{||} = 2.22$ lines with a concomitant increase in intensity of a new low field set of lines. At pH 5.95, individual peaks are difficult to assign in the parallel region due to the presence of broad overlapping signals, indicating that several species are present. At pH 5.55, the spectrum has four dominant peaks with $g_{||} = 2.41$ and $A_{||} = 408$ MHz (121 G), which is characteristic of aqueous copper. The spectrum of a control Cu^{2+} sample at pH 4.00 is shown at the bottom of Figure 5 for reference. Although the parallel region of the spectrum of rPrP at pH 5.55 is indicative of aqueous copper, the differences in $g_\perp$ region demonstrate that a small amount of Cu^{2+} may still be bound to the protein. Thus, full-length rPrP releases the majority of its Cu^{2+} by pH 5.55. A similar pH-dependence for Cu^{2+}-binding was observed for PrP(23−28, 57−91) (*9*).

EPR Spectra of the Copper Site Outside of the Octarepeat Domain. The library of PrP-derived peptides was further examined to search for the additional C-terminal copper-binding site in the flexible region, approximately residues 90−128, that intervenes between the octarepeat domain and the well-ordered globular, C-terminal domain. Spectra obtained from PrP(90−116) at pH 7.4 as a function of added Cu^{2+} are shown in Figure 6. At 0.5 equiv Cu^{2+}, the spectrum is very similar to that of rSHaPrP(90−231) with 1 equiv of Cu^{2+}. Superhyperfine splitting is observable in the $g_\perp$ region. Upon further addition of Cu^{2+}, the high field peak decreases in intensity with loss of resolution of the prominent negative doublet between 3300 and 3400 G.

The peptides PrP(90−101) and PrP(106−116) represent N-terminal and C-terminal segments of PrP(90−116), respectively, where each segment contains a single histidine. The three peptides were examined in the presence of excess copper and the EPR spectra are shown in Figure 7. The spectrum obtained from PrP(90−101) is nearly identical to

FIGURE 4: Schematic of full-length PrP with the sequence of the octarepeat and other important regions included. Aligned directly below are the PrP-derived protein and peptide segments used in this study. The Cu^{2+} binding stoichiometry for each protein or peptide is given on the left. *These peptides are capable of binding an additional equivalent of Cu^{2+} at high copper concentrations, thus indicating site(s) with low affinity.

Table 2: Cu^{2+} Binding Stoichiometries of Proteins and Peptides Determined by EPR

protein or peptide	equiv Cu^{2+} bound determined by EPR[a]
rSHaPrP(29−231)	5.3 ± 1.1
rSHaPrP(90−231)	0.8 ± 0.2[b]
PrP(23−28,57−98)	5.2 ± 1.0
PrP(23−28,57−91)	3.8 ± 0.8
PrP(90−116)	0.8 ± 0.2[b]
PrP(90−101)	1.1 ± 0.2
PrP(106−116)	0.7 ± 0.1
PrP(92−96)	0.8 ± 0.2

[a] Error from spin integration, protein concentration determination, and pipetting is estimated at 20%. Except where noted, values were determined by either titration or by quantitative signal integration after addition of excess copper. [b] These constructs can take up an additional copper if the metal ion is added at several-fold excess. The binding stoichiometry reported was determined with 1.0 equiv added Cu^{2+}.

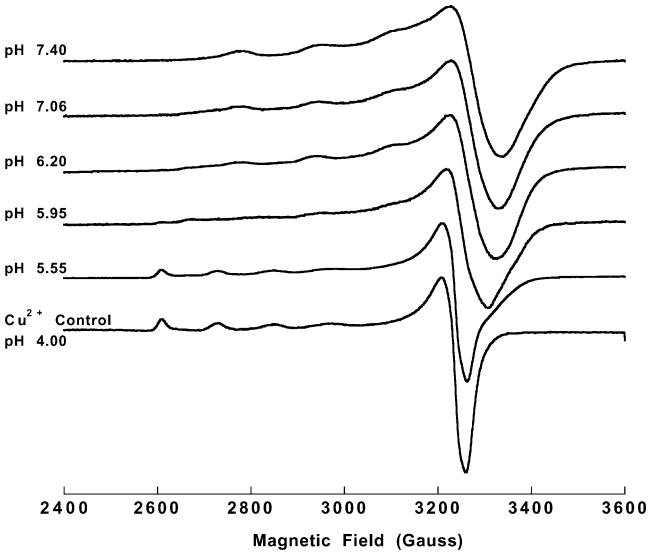

FIGURE 5: X-band EPR spectra of 39 μm rMoPrP at pH values ranging from 7.40 to 5.55. (Note: mouse PrP was used due to availability; sequence differences in the copper binding regions between the mouse and hamster sequences are minor.) The spectrum of aqueous Cu^{2+} at pH 4.00 is shown at bottom for reference. Spectra collected at 85 K, υ_0 = 9.43 GHz, and a sweep width of 1200 G.

that of PrP(90−116) with 0.5 equiv of Cu^{2+} (Figure 6), and rSHaPrP(90−231) with 1 equiv of Cu^{2+}. The only noticeable difference is that PrP(90−101) has significant resolvable

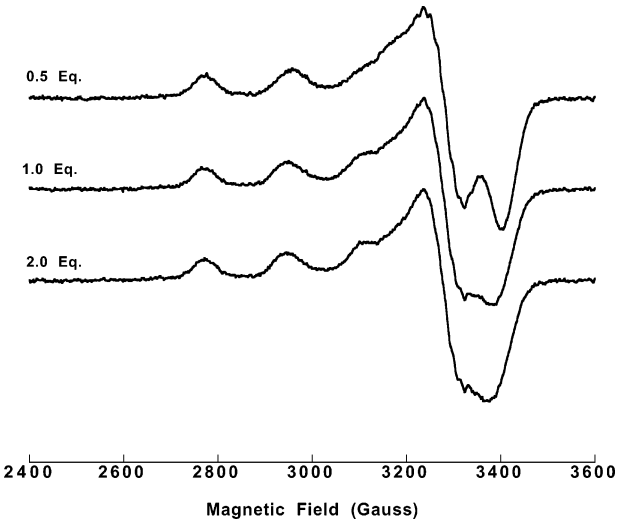

FIGURE 6: X-band EPR spectra of PrP(90−116) with indicated equivalents of Cu^{2+} at pH 7.4. Spectra collected at 85 K, υ_0 = 9.43 GHz, and a sweep width of 1200 G.

superhyperfine splittings in the $g_\perp$ region. Alternatively, the spectrum of PrP(106−116) is distinct from the previous three in Figure 7. A 1:1 sum of the spectra of PrP(90−101) and PrP(106−116) yields a spectrum (not shown) nearly identical to that of PrP(90−116), demonstrating that there are two distinct binding sites at high copper concentration.

The EPR spectrum of PrP(92−96), which corresponds to the residues GGGTH, is identical to that of PrP(90−101) and thus further identifies the copper ion binding site. Here, even the ligand superhyperfine splittings match exactly. Last, the tripeptide GTH exhibits a spectrum that shares similarities in the $g_{||}$ region but has significant differences in the $g_\perp$ region when compared to PrP(90−116) and PrP(92−96). Because spectra of this tripeptide did not match that of the longer constructs, detailed spin integration was not pursued.

Magnetic parameters obtained from the spectra displayed are reported in Table 3. According to the Peisach-Blumberg tables, the $g_{||}$ and $A_{||}$ values for PrP(92−96) are in the range expected for equatorial coordination of three nitrogen ligands and one oxygen ligand (3N 1O) or four nitrogen ligands (4N) (*29*). Superhyperfine couplings can also provide information about the number of nitrogen ligands around a Cu^{2+} atom. Nitrogens directly coordinated to Cu^{2+} typically have couplings between 10 and 15 G (*30*, *31*). The spectra of both

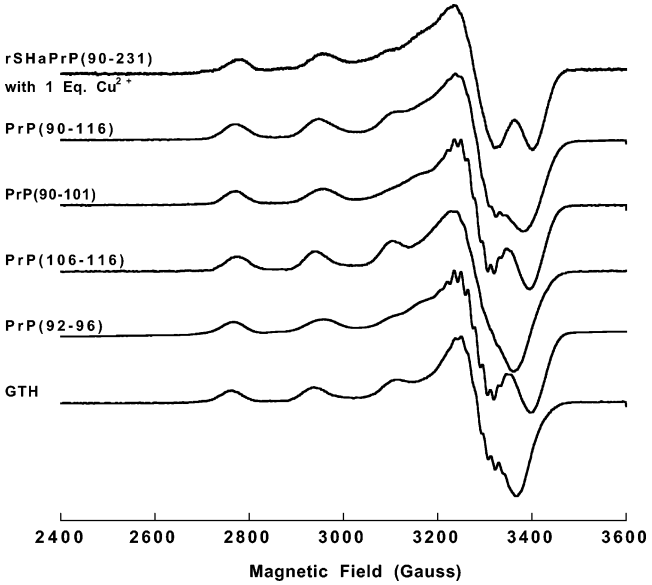

FIGURE 7: X-band EPR spectra of rSHaPrP(90−231) with 1 equiv of Cu^{2+} plus PrP(90−116), PrP(90−101), PrP(106−116), PrP(92−96), and GTH all with excess Cu^{2+}, at pH 7.4. Spectra collected at 85 K, $\upsilon_0 = 9.43$ GHz, and a sweep width of 1200 G.

Table 3: EPR Parameters for All Cu^{2+} Complexes at pH 7.47 ± 0.06

		$A_{\|}$[b]	
sequence	$g_{\|}$[a]	MHz	(G)
rSHaPrP(29−231)[c]	2.22	541	(174)
rSHaPrP(90−231)[c]	2.22	541	(174)
PrP(23−28,57−98)	2.23	493	(158)
PrP(23−28,57−91)	2.23	493	(158)
PrP(90−116)	2.22	544	(175)
PrP(90−101)	2.21	588	(190)
PrP(106−116)	2.23	518	(166)
PrP(92−96)	2.21	588	(190)
PrP(94−96)	2.23	562	(180)

[a] The error in all reported g values is less than ± 0.01. [b] Error in A values ± 6 MHz (± 2 G). [c] Values reported for dominant spectral feature.

PrP(90−101) and PrP(92−96) reveal at least eight discernible lines with splittings of 16 ± 1 G. This supports the above assignment that at least three nitrogens coordinate Cu^{2+}.

Upon closer examination, peptides PrP(90−101) and PrP(92−96) reveal an additional feature at 3150 G suggestive of two coexisting species. Because Cu^{2+} binding is highly pH dependent, all of the peptides of Figure 7 were examined from pH 7.2 to nearly 8.0 and PrP(90−231) was examined from 7.2 to 7.5 (data not shown). Indeed, at pH approaching 8.0, a new spectrum characterized by larger $A_{\|}$ values (∼200 G) emerges. The presence of this species explains the anomalously large values of $A_{\|}$ measured for PrP(90−101) and PrP(92−96) in Table 3. While the model peptides are quite sensitive to pH, the spectrum of PrP(90−231) does not vary significantly over the pH range tested. Despite the agreement between PrP(90−231) and peptides containing residues 92−96, the differential behavior as a function of pH suggests that the peptides are imperfect models and that the full PrP C-terminal domain offers additional stabilizing features in its nonoctarepeat binding site. Because the second species observed in the peptides does not dominate below pH 8.0, at this juncture, we do not believe it is physiologically relevant. Further work will be needed to determine the exact nature of this component.

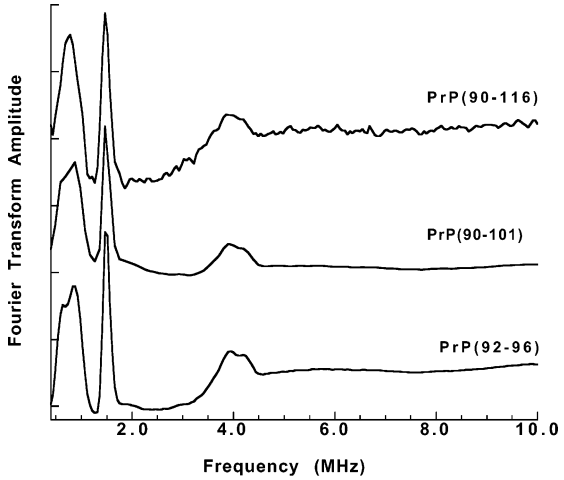

FIGURE 8: Three-pulse ESEEM spectra for Cu^{2+}-loaded PrP(90−116), PrP(90−101), and PrP(92−96) at pH 7.4 obtained at X-band. Spectra were obtained at 4.2 K from the $g_{\perp}$ region of the spectrum with $\tau = 150$ ns.

ESEEM and S-Band EPR. The X-band EPR studies above indicate that the high affinity C-terminal binding site is contained within the sequence GGGTH. To aid in identification of the specific contacts involved in Cu^{2+} coordination, three-pulse ESEEM spectroscopy was performed (*32*, *33*). ESEEM spectroscopy is a pulsed EPR technique that detects spin-active nuclei within approximately 10 Å from a paramagnetic center. For copper, ESEEM transitions arise from ^{14}N nuclei that are not directly coordinated to this center. This technique is ideal for identifying imidazole coordination via detection of the remote nitrogen. We found that the solubility limit for the Cu^{2+}-loaded, full-length recombinant PrP at pH 7.4 is below the detection limit for ESEEM spectroscopy, but the technique can be used to examine the PrP-derived peptides. Spectra for fully Cu^{2+}-loaded PrP(90−116), PrP(90−101), and PrP(92−96) are shown in Figure 8. The spectra are nearly identical and have features that are characteristic of coordination by a single histidine imidazole. In addition, the three peptides gave similar modulation amplitudes in the time domain (data not shown), indicating that the same number of imidazoles in each case coordinates copper. This finding, in conjunction with the lack of combination lines, which should arise in the case of multiple histidine coordination, is indicative of single imidazole binding to each copper in the 90−116 region.

To further investigate the possibility of multiple His coordination, ESEEM spectra were obtained at multiple τ values (140−240 ns in 20-ns increments) to determine whether the absence of combination bands was from signal suppression characteristic of the three-pulse experiment. Examination of the spectra (data not shown) did not reveal any new spectral features. Moreover, the ratio of the modulation amplitude to the total echo amplitude remained constant in time domain data. We do note, in Figure 8, two very weak absorption signals at approximately 2.0 and 3.0 MHz. While these likely arise from single quantum transitions in the noncanceled electron spin manifold, we cannot rule out weak coupling from a neighboring nonbonded nitrogen. Regardless, these weak signals are unlikely to arise

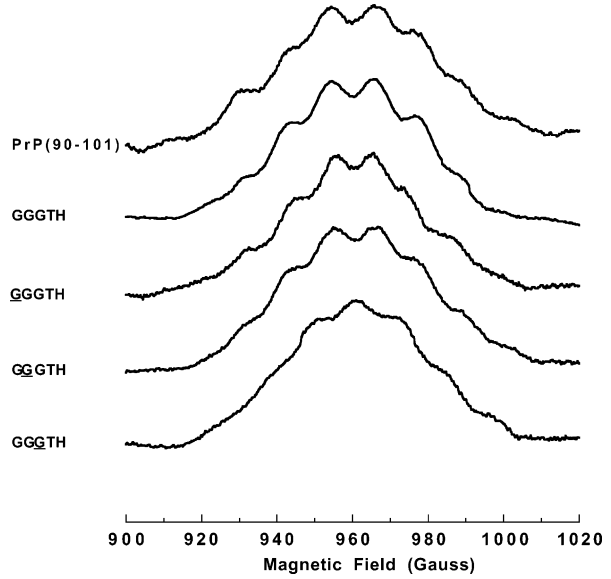

FIGURE 9: The $m_I = -1/2$ line from S-band EPR (3.5 GHz) of Cu^{2+}-loaded PrP(90−101), GGGTH, and ^{15}N-labeled GGGTH peptides at 133 K. ^{15}N-labeled amino acids are underlined. For GGGTH, a change in multiplet structure is only observed when the last glycine is ^{15}N-labeled, demonstrating that this nitrogen coordinates Cu^{2+}.

from multiple His coordination since they are seen in all three peptides of which only one has two His residues (PrP(90−116)). Finally, we note that ESEEM were recorded at various pH values to determine whether the two coexisting species observed in Figure 7 had different His coordination profiles. However, no pH dependence was observed. Taken together, these findings strongly suggest that Cu^{2+} coordination in PrP(90−231) involves only His96.

The X-band spectra of PrP(90−101) and GGGTH both revealed superhyperfine splittings indicative of coupling to more than a single nitrogen atom. In addition to the nitrogen atoms of histidine imidazoles, deprotonated amide nitrogens may also participate in Cu^{2+} coordination. To determine which additional nitrogen atoms beyond that from the imidazole bind Cu^{2+}, both PrP(90−101) and GGGTH, plus a series of sequentially labeled ^{15}N-labeled analogues of GGGTH, were examined by S-band EPR. Low frequency S-band (3.4 GHz) EPR is excellent for clearly resolving nitrogen couplings. The improvement in spectral resolution for S-band over X-band EPR arises from a partial cancellation of *g*-strain− and *A*-strain−induced inhomogeneous broadening for specific hyperfine lines. At S-band, this cancellation selectively narrows the $m_I = -1/2$ hyperfine line (*30*). Since ^{15}N has a spin $I = 1/2$, a change in the multiplet pattern is observed if that nitrogen coordinates copper (*9*, *10*).

S-band spectra of the $^{63}Cu^{2+}$ $m_I = -1/2$ line are shown for PrP(90−101), GGGTH, and the GGGTH ^{15}N-analogues in Figure 9. Spectra for PrP(90−101) and GGGTH are equivalent, each showing a splitting pattern consisting of eight or more resolved lines, and, consistent with the ESEEM and X-band spectra, suggest that each construct coordinates copper in an equivalent fashion. Inspection of spectra from the ^{15}N-labeled peptides reveals an isotope influence only for the third glycine amide, demonstrating that its amide nitrogen directly coordinates Cu^{2+}. The S-band spectra also reveal an even number of superhyperfine lines (except for GGGTH). If the multiplet was due solely to equivalent ^{14}N interactions, one should observe an odd multiplet pattern. An even multiplet can arise from inequivalent ^{14}N superhyperfine interactions or an additional $I = 1/2$ spin, possibly from a nearby proton. In most cases, there is only small variance in the magnitude of hyperfine couplings for directly coordinated nitrogen atoms. Alternatively, there is good precedent for proton coupling to metal centers (see discussion in ref *9*). Since all S-band spectra were obtained in D_2O solution, an ^1H coupling likely arises from a nonexchangeable proton within the peptide.

As reported previously (*9*), S-band spectra of PrP(23−28,57−91) produced no observable splittings. It is possible that inhomogeneous broadening masks the multiplet pattern. Given that fully loaded PrP(23−28,57−91) contains four Cu^{2+} ions, weak dipolar interactions between the paramagnetic centers may contribute an additional source of inhomogeneous broadening that is not canceled in the $m_I = -1/2$ line at S-band. Unfortunately, solubility limitations prevented us from examining rSHaPrP(29−231) and rSHaPrP(90−231).

DISCUSSION

The findings reported here demonstrate that rSHaPrP(29−231) takes up approximately five copper ions in its fully loaded state. The protein takes up a sixth copper only if the metal ion is added in significant excess. Comparing the copper stoichiometry of rSHaPrP(29−231) and rSHaPrP(90−231) shows that four equivalents are in the octarepeat domain, composed of four PHGGGWGQ segments, and the fifth copper binds beyond residue 90. rSHaPrP(29−231) was evaluated for its ability to bind copper as a function of pH. As found previously for peptides corresponding to the octarepeat domain, the full-length protein is only able to bind copper above pH 6.0. That rSHaPrP(29−231) takes up four coppers in its octarepeat domain and exhibits spectral features and pH sensitivity almost identical to the construct PrP(23−28,57−91) argues that the previously identified octarepeat binding mode (*10*) applies to the full-length protein. Next, using a series of PrP-derived peptides, the fifth copper site was localized to His96. This newly identified site was further characterized using a series of peptides in conjunction with X-band EPR, S-band EPR, and ESEEM. Here we find that copper is coordinated by three to four nitrogens, in which one is from the imidazole of His96 and another is from the amide nitrogen of Gly94.

The stoichiometric findings here agree well with other studies (*5*, *7*, *12*, *13*). The localization of the five main Cu^{2+} binding sites in full-length rSHaPrP to the individual PHGGGWGQ segments of the octarepeat region and to GGGTH also agrees remarkably well with diethylpyrocarbonate (DEPC) protection experiments on full-length rMoPrP by Qin et al. (*13*). This study showed that Cu^{2+} binds to histidine residues 61, 69, 77, 85, 96 (note, here the sequence numbering has been translated from the MoPrP reference frame to the SHaPrP frame), i.e., all four His residues in the octarepeat region and the adjacent GGGTH region. Their work further illustrates that any additional Cu^{2+} binding above five equivalents per rPrP is most likely nonspecific and not physiologically relevant, consistent with our findings here.

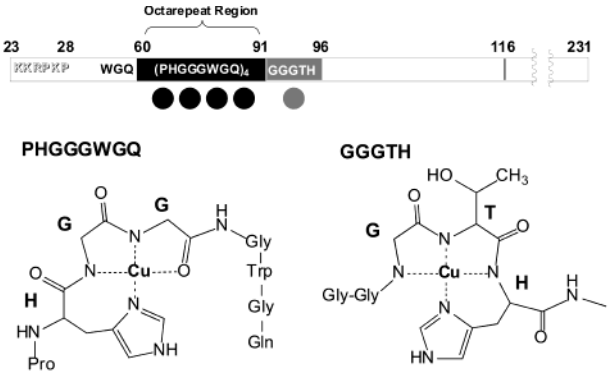

FIGURE 10: Location of the five main Cu^{2+} binding sites along the rSHaPrP sequence, top. Bond-line models of the equatorial Cu^{2+} coordination sphere for the two different types of binding are shown below. The structure for the single HGGGW−Cu^{2+} unit was determined from crystallographic and spectroscopic data (*10*). This structure is maintained for each HGGGW unit in the full octarepeat region. The coordination sphere depicted for GGGTH−Cu^{2+} is a model based on data discussed in this work.

Previously, we established the Cu^{2+} coordination sphere in the octarepeat region using a combination of EPR and crystallographic methods (*10*). The crystal structure of the HGGGW−Cu^{2+} complex reveals a pentacoordinate environment with equatorial ligation from the δ1 nitrogen of the His imidazole and deprotonated amide nitrogens from the next two Gly residues. The second Gly also contributes its amide carbonyl oxygen. In an analogous fashion, this current work has now narrowed in on another segment of PrP responsible for Cu^{2+} binding, specifically GGGTH (i.e., residues 92−96).

The peptide GGGTH binds approximately one equivalent of Cu^{2+} and the EPR splitting parameters indicate that 4N or 3N 1O comprise the equatorial coordination sphere. ESEEM spectroscopy demonstrates the coordination of a single histidine with no evidence of any other weakly coupled nitrogens. Scanning ^{15}N through the glycines demonstrates that the third Gly amide (GG<u>G</u>TH) participates in equatorial coordination. Either one or both amide nitrogens of Thr−His also bind Cu^{2+}. Interestingly, an amide nitrogen ESEEM signal is observed in the case of the octarepeat sequence HGGGW because carbonyl ligation places the nitrogen of the following residue approximately 4 Å from the copper. If just one of the Thr or His amide nitrogens coordinated Cu^{2+}, the remaining noncoordinated nitrogen would be held in similar close proximity to the paramagnetic center, thus giving rise to an ESEEM signal. However, as discussed, such a signal is not observed (Figure 8). Thus, we believe it is unlikely that an oxygen ligand is supplied by a backbone carbonyl. Amide binding by both Thr and His, which is ESEEM silent, or aquo binding, is a more likely scenario. Taken together, we propose a working hypothesis for copper binding in the GGGTH segment in Figure 10. Figure 7 shows that GTH alone does not provide the necessary coordination environment and that the first two glycines in the GGGTH segment are required to give a spectrum equivalent to that of rSHaPrP(90−231). However, the first two glycines do not participate in equatorial coordination. It is possible that one of these nonequatorial glycines coordinates in an axial position analogous to the role of Trp in the HGGGW sequence of each octarepeat. Alternatively, the extra glycines may create steric hindrance, thereby preventing formation

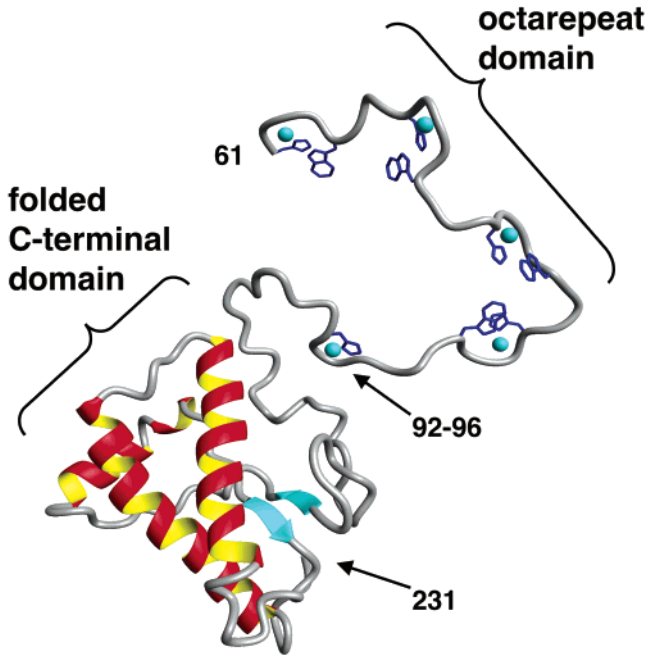

FIGURE 11: Three-dimensional rendering of PrP(61−231) with coppers included. Crystal structure coordinates were used for the octarepeat binding units HGGGW. The PrP(92−96) segment is based on the model shown in Figure 10. Intervening regions were built in a relaxed conformation. Coordinates for PrP(97−231) were provided by T. L. James.

of a bis peptide complex. Further work will be required to clarify this issue. Figure 10 also shows the previously determined equatorial binding mode for the HGGGW octarepeat segments. To put our cumulative findings in perspective, a rendering of PrP(61−231) corresponding to the folded C-terminal domain and the copper-binding domain is shown in Figure 11. All histidines are shown, as are the octarepeat tryptophans that interact with axially coordinated water molecules (*10*). At this time, how the individual copper binding segments organize relative to each other and how the overall domain orients with respect to the folded C-terminal domain is unknown. Thus, relaxed conformations were assumed for residues 97−112 as well as the Gly−Gln−Pro (GQP) residues intervening between the copper sites. Interestingly, recent CD difference spectroscopy studies suggest specific structuring of the GQP octarepeat linkers (*34*) perhaps consistent with a partially extended structure. In our model, the prolines tend to introduce turns between the octarepeats, whereas the linker between the most C-terminal octarepeat and the last binding site at the C-terminal end of this region is likely to be flexible and extended. That this region binds copper in a cooperative fashion suggests there may be additional folded structure in this domain not yet revealed by our studies.

The binding site outside of the octarepeat domain is significant not only because it coordinates Cu^{2+} under physiological conditions but also because it is linked to the ability of the octarepeat region to bind Cu^{2+} cooperatively. At least two studies have shown that extending the sequence from 91 to at least residue 98 markedly increases the affinity of the entire octarepeat region for Cu^{2+} (*5*, *12*). The sequence 60−98 binds Cu^{2+} in a cooperative manner that is nearly identical to that of full-length PrP and can account for the binding of five Cu^{2+} atoms. Adding amino acids beyond this

has only a minor effect on the affinity. Thus, the sequence GGGTH should be considered an integral part of PrP's copper-binding domain.

In light of the role played by the nonoctarepeat binding site, it is interesting to note that this site coordinates copper in a fashion quite distinct from the octarepeat HGGGW sequence. In the nonoctarepeat site, Cu^{2+} interacts with backbone amides on the N-terminal side of His96, whereas in the octarepeat sites, the metal ion is directed toward the C-terminal side of each respective His (Figure 10). Typically, N-terminal coordination is preferred as observed in both model peptides and proteins (*35*). Recent theoretical studies by Pushie and Rauk identified the 3N 1O Cu^{2+} coordination in HGGGW, observed in our crystallographic and EPR work, as the lowest energy configuration (*36*). On the basis of their computational findings, the authors further suggested that the octarepeat prolines serve as break points, thus directing the observed C-terminal coordination in the octarepeat domain. Consistent with this suggestion, CD studies by Garnett and Viles demonstrate that replacement of the Pro with Ala in octarepeat peptides leads to a fundamental change in the Cu^{2+} binding environment (*34*). Consequently, the prolines may serve to tune PrP's copper affinity in the octarepeat domain. Taken together, these findings point toward a sequential model of Cu^{2+} uptake in which the higher affinity at His96 site takes up the first copper ion and then facilitates cooperative uptake in the adjacent octarepeat domain.

Two recent publications have proposed fundamentally different PrP/copper interactions than that identified here. Jackson et al. studied Cu^{2+} binding to human PrP(52−98) and PrP(91−231) in the presence of a competitive glycine buffer (*37*). Using fluorescence spectroscopy, they deduced the presence of two copper binding sites. One site consisted of four of the five His imidazoles in 52−98, with a K_d of $\sim 10^{-14}$, and a second site was found around histidines 96 and 111 with a slightly higher K_d. Copper coordination by four imidazoles would yield remarkable ESEEM combination peaks which were not observed in our studies of PrP(23−28,57−91) (*9*, *10*). Hasnain et al. refined the features of the second site identified by Jackson et al. with XAFS studies on PrP(91−231) (*38*). On the basis of the 1:1 Cu^{2+}/PrP(91−231) stoichiometry, they proposed that the histidine coordination to the single copper must result from two imidazoles, His96 and His111. With regard to this site, our ESEEM spectra of PrP(90−116) (Figure 8) lacks the combination peaks and the increased modulation amplitude expected for multiple histidine coordination. In addition, titration of SHaPrP(90−231) shows that the signature assigned to 92−96 dominates with one equivalent of copper. Jackson et al. raise an important issue that evaluation of a relevant copper affinity must take into account the specific buffer conditions. However, we are unable to reconcile the molecular features of their proposed binding sites with our spectroscopic data.

Our findings as well as those of Qin et al. (*13*) may have bearing on the role of copper in the development of prion disease. The octarepeat domain is outside of the protease-resistant core of infectious PrP^{Sc}, corresponding to PrP(90−231) in hamster (*1*). In addition, PrP-knockout mice possessing a transgene that produces PrP devoid of residues 32−93 retain their susceptibility to prion infection although with longer incubation times (*39*). It is clear now, however, that copper binding takes place outside of the octarepeats and thus may be a cofactor in the production of PrP^{Sc}. Indeed, recent studies show that addition of copper to PrP^{C} converts the protein to a partially protease-resistant state, and this conversion requires only a single copper binding site (*40*).

The normal physiological role of PrP^{C} is currently unknown, but some recent studies point toward an antioxidant function. Among the specific theories are that PrP^{C} is (i) a superoxide dismutase (SOD) (*16*), (ii) a transmembrane copper transporter that operates through endocytosis (*5*, *10*, *14*), and (iii) a copper buffer that sequesters excess metal ion at the plasma membrane (*41*). SOD activity requires that the copper ion have two accessible oxidation states to complete the dismutation cycle. In known copper-dependent SODs, this involves Cu^{+} and Cu^{2+} (*42*). Although Cu^{2+} readily coordinates to deprotonated amide bonds, as shown here and in our previous work, this is not the case for Cu^{+} (*35*). Consequently, the binding sites identified in our studies will likely not coordinate Cu^{+} as required for SOD function. This does not rule out an SOD function for PrP^{C} but does suggest that the copper-binding domain would have to significantly restructure to support this activity. Yet another possibility is that copper alternates between the Cu^{2+} and Cu^{3+} oxidation states, although this is unlikely.

Several labs have now investigated the potential for copper transport function. In general, these studies have failed to find direct evidence that copper transport depends on the level of PrP expression (*15*, *41*).

Quite recently, evidence has emerged suggesting that PrP^{C} plays a protective role against deleterious redox activity by sequestering excess Cu^{2+} (*41*). Wild-type cells are more resistant to oxidative stress, relative to PrP knockouts, and concentrate copper at the plasma membrane (*41*). In turn, this suggests that PrP^{C} functions as part of a "cuprostat" that helps maintain neuron integrity in the copper-rich environment of the central nervous system. The PrP^{C} structure identified in our work (Figure 11) readily takes up copper at extracellular pH and is fully consistent with this function. Numerous papers have speculated that loss of PrP^{C} function in the TSEs is partly responsible for neurodegeneration (e.g., see refs *16* and *18*). With regard to cuprostat function, interesting new results indeed demonstrate that cultured cells infected with PrP^{Sc} are more susceptible to oxidative stress and exhibit a significant reduction in the ability to bind copper despite maintaining normal PrP levels (*43*).

In summary, these studies combine peptide design with EPR, ESEEM, and titration experiments to evaluate the Cu^{2+} binding sites in full-length recombinant prion protein, SHaPrP(29−231). Previous spectroscopic studies by our lab utilized PrP-derived peptides. Our findings here demonstrate that the mode of copper coordination identified by these studies holds in the full-length protein. In addition, we have characterized an additional binding site and provided a preliminary model of its molecular features. The latter site is relevant as it plays a significant role in the cooperative nature of copper uptake. These studies continue to demonstrate that PrP binds copper in a highly pH-dependent fashion, a finding that supports the hypothesis that PrP's function is related to its ability to bind copper selectively when presented to the extracellular milieu. How PrP takes up copper in a cooperative fashion, how copper transduces a signal for endocytosis, and how copper produces a protease-

resistant state are only a few of the fundamental questions yet to be addressed.

REFERENCES

1. Prusiner, S. B. (1998) *Proc. Natl. Acad. Sci. U.S.A. 95*, 13363−13383.
2. Prusiner, S. B. (1997) *Science 278*, 245−251.
3. Kocisko, D. A., Priola, S. A., Raymond, G. J., Chesebro, B., Landsbury, P. T. J., and Caughey, B. (1995) *Proc. Natl. Acad. Sci. U.S.A. 92*, 3923−3927.
4. Scott, M. R., Will, R., Ironside, J., Nguyen, H. O., Tremblay, P., DeArmond, S. J., and Prusiner, S. B. (1999) *Proc. Natl. Acad. Sci. U.S.A. 96*, 15137−15142.
5. Whittal, R. M., Ball, H. L., Cohen, F. E., Burlingame, A. L., Prusiner, S. B., and Baldwin, M. A. (2000) *Protein Sci. 9*, 332−343.
6. Brown, D. R., Qin, K., Herms, J. W., Madlung, A., Manson, J., Strome, R., Fraser, P. E., Kruck, T., von Bohlen, A., Schulz-Schaeffer, W., Giese, A., Westway, D., and Kretzschmar, H. (1997) *Nature 390*, 684−687.
7. Hornshaw, M. P., McDermott, J. R., and Candy, J. M. (1995) *Biochem. Biophys. Res. Commun. 207*, 621−629.
8. Miura, T., Hori-i, A., Mototani, H., and Takeuchi, H. (1999) *Biochemistry 38*, 11560−11569.
9. Aronoff-Spencer, E., Burns, C. S., Avdievich, N. I., Gerfen, G. J., Peisach, J., E., A. W., Ball, H. L., Cohen, F. E., Prusiner, S. B., and Millhauser, G. L. (2000) *Biochemistry 39*, 13760−13771.
10. Burns, C. S., Aronoff-Spencer, E., Dunham, C. M., Lario, P., Avdievich, N. I., Antholine, W. E., Olmstead, M. M., Vrielink, A., Gerfen, G. J., Peisach, J., Scott, W. G., and Millhauser, G. L. (2002) *Biochemistry 41*, 3991−4001.
11. Stöckel, J., Safar, J., Wallace, A. C., Cohen, F. E., and Prusiner, S. B. (1998) *Biochemistry 37*, 7185−7193.
12. Kramer, M. L., Kratzin, H. D., Schmidt, B., Romer, A., Windl, O., Liemann, S., Hornemann, S., and Kretzschmar, H. (2001) *J. Biol. Chem. 276*, 16711−16719.
13. Qin, K., Yang, Y., Mastrangelo, P., and Westaway, D. (2002) *J. Biol. Chem. 277*, 1981−1890.
14. Pauly, P. C., and Harris, D. A. (1998) *J. Biol. Chem. 273*, 33107−33119.
15. Waggoner, D. J., Drisaldi, B., Bartnikas, T. B., Casareno, R. L. B., Prohaska, J. R., Gitlin, J. D., and Harris, D. A. (2000) *J. Biol. Chem. 275*, 7455−7458.
16. Brown, D. R., Wong, B.-S., Hafiz, F., Clive, C., Haswell, S. J., and Jones, I. M. (1999) *Biochem. J. 344*, 1−5.
17. Klamt, F., Dal-Pizzol, F., Conte da Frota, M. L., Jr., Walz, R., Andrades, M. E., da Silva, E. G., Brentani, R. R., Izquierdo, I., and Fonseca Moreira, J. C. (2001) *Free Radical Biol. Med. 30*, 1137−1144.
18. Brown, D. R. (2001) *Trends Neurosci. 24*, 85−90.
19. Zahn, R., Liu, A., Luhrs, T., Riek, R., von Schroetter, C., Lopez Garcia, F., Billeter, M., Calzolai, L., Wider, G., and Wuthrich, K. (2000) *Proc. Natl. Acad. Sci. U.S.A. 97*, 145−150.
20. Riek, R., Hornemann, S., Wider, G., Billeter, M., Glockshuber, R., and Wuthrich, K. (1996) *Nature 382*, 180−182.
21. Riek, R., Hornemann, S., Wider, G., Glockshuber, R., and Wuthrich, K. (1997) *FEBS Lett. 413*, 282−288.
22. Donne, D. G., Viles, J. H., Groth, D., Mehlhorn, I., James, T. L., Cohen, F. E., Prusiner, S. B., Wright, P. E., and Dyson, H. J. (1997) *Proc. Natl. Acad. Sci. U.S.A. 94*, 13452−13456.
23. Viles, J. H., Cohen, F. E., Prusiner, S. B., Goodin, D. B., Wright, P. E., and Dyson, H. J. (1999) *Proc. Natl. Acad. Sci. U.S.A. 96*, 2042−2047.
24. Bonomo, R. P., Impellizzeri, G., Pappalardo, G., Rizzarelli, E., and Tabbi, G. (2000) *Chem. Eur. J. 6*, 4195−4202.
25. Mehlhorn, I., Groth, D., Stockel, J., Moffat, B., D., R., Yansura, D., Willett, W. S., Baldwin, M., Fletterick, R., Cohen, F. E., Vandlen, R., Henner, D., and Prusiner, S. B. (1996) *Biochemistry 35*, 5528−5537.
26. Jiang, F., McCraken, J., and Peisach, J. (1990) *J. Am. Chem. Soc. 112*, 9035−9044.
27. Bender, C. J., Casimiro, D. R., Peisach, J., and Dyson, H. J. (1997) *J. Chem. Soc., Faraday Trans. 93*, 3967−3980.
28. Cornelius, J. B., McCracken, J., Clarkson, R. B., Belford, R. L., and Peisach, J. (1990) *J. Phys. Chem. 94*, 6977−6982.
29. Peisach, J., and Blumberg, W. E. (1974) *Arch. Biochem. Biophys. 165*, 691−708.
30. Froncisz, W., and Hyde, J. S. (1980) *J. Phys. Chem. 73*, 3123−3131.
31. Yuan, H., Antholine, W. E., and Kroneck, P. M. H. (1998) *J. Inorg. Biochem. 71*, 99−107.
32. Mims, W. B., and Peisach, J. (1978) *J. Chem. Phys. 69*, 4921−4930.
33. Mims, W. B., and Peisach, J. (1981) in *Biological Magnetic Resonance* (Berliner, L. J., and Reuben, J., Eds.), Plenum Press, New York.
34. Garnett, A. P., and Viles, J. H. (2003) *J. Biol. Chem. 278*, 6795−802.
35. Kroneck, P. M., Vortisch, V., and Hemmerich, P. (1980) *Eur. J. Biochem. 109*, 603−12.
36. Pushie, M. J., and Rauk, A. (2003) *J. Biol. Inorg. Chem. 8*, 53−65.
37. Jackson, G. S., Murray, I., Hosszu, L. L. P., Gibbs, N., Waltho, J. P., Clarke, A. R., and Collinge, J. (2001) *Proc. Natl. Acad. Sci. U.S.A. 98*, 8531−8535.
38. Hasnain, S. S., Murphy, L. M., Strange, R. W., Grossmann, J. G., Clarke, A. R., Jackson, G. S., and Collinge, J. (2001) *J. Mol. Biol. 311*, 467−473.
39. Flechsig, E., Shmerling, D., Hegyi, I., Raeber, A. J., Fischer, M., Cozzio, A., von Mering, C., Aguzzi, A., and Weissmann, C. (2000) *Neuron 27*, 399−408.
40. Quaglio, E., Chiesa, R., and Harris, D. A. (2001) *J. Biol. Chem. 276*, 11432−8.
41. Rachidi, W., Vilette, D., Guiraud, P., Arlotto, M., Riondel, J., Laude, H., Lehmann, S., and Favier, A. (2003) *J. Biol. Chem. 278*, 9064−9072.
42. Lippard, S. J., and Berg, J. M. (1994) *Principles of Bioinorganic Chemistry*, University Science Books, Mill Valley, Calif.
43. Rachidi, W., Mange, A., Senator, A., Guiraud, P., Riondel, J., Benboubetra, M., Favier, A., and Lehmann, S. (2003) *J. Biol. Chem*. Papers in Press, March 10, 2003, manuscript C300092200.

BI027138+